Bandgap narrowing in the layered oxysulfide semiconductor $Ba_3Fe_2O_5Cu_2S_2$: Role of FeO_2 layer*

Han Zhang(张韩)[1], Shifeng Jin(金士锋)[1,†], Liwei Guo(郭丽伟)[1], Shijie Shen(申士杰)[1], Zhiping Lin(林志萍)[1], and Xiaolong Chen(陈小龙)[1,2]

[1] *Research and Development Center for Functional Crystals, Beijing National Laboratory for Condensed Matter Physics, Institute of Physics, Chinese Academy of Sciences, Beijing* 100190, *China*

[2] *Collaborative Innovation Center of Quantum Matter, Beijing, China Research & Development Center for Functional Crystals, Beijing National Laboratory for Condensed Matter Physics, Institute of Physics, Chinese Academy of Sciences, Beijing* 100190, *China*

(Received 19 October 2015; revised manuscript received 1 December 2015; published online 10 January 2016)

A new layered Cu-based oxychalcogenide $Ba_3Fe_2O_5Cu_2S_2$ has been synthesized and its magnetic and electronic properties were revealed. $Ba_3Fe_2O_5Cu_2S_2$ is built up by alternatively stacking $[Cu_2S_2]^{2-}$ layers and iron perovskite oxide $[(FeO_2)(BaO)(FeO_2)]^{2-}$ layers along the *c* axis that are separated by barium ions with Fe^{3+} fivefold coordinated by a square-pyramidal arrangement of oxygen. From the bond valence arguments, we inferred that in layered Cu*Ch*-based (*Ch* = S, Se, Te) compounds the +3 cation in perovskite oxide sheet prefers a square pyramidal site, while the lower valence cation prefers the square planar sites. The studies on susceptibility, transport, and optical reflectivity indicate that $Ba_3Fe_2O_5Cu_2S_2$ is an antiferromagnetic semiconductor with a Néel temperature of 121 K and an optical bandgap of 1.03 eV. The measurement of heat capacity from 10 K to room temperature shows no anomaly at 121 K. The Debye temperature is determined to be 113 K. Theoretical calculations indicate that the conduction band minimum is predominantly contributed by O 2p and 3d states of Fe ions that antiferromagnetically arranged in FeO_2 layers. The Fe 3d states are located at lower energy and result in a narrow bandgap in comparison with that of the isostructural $Sr_3Sc_2O_5Cu_2S_2$.

Keywords: oxychalcogenides, semiconductor, antiferromagnetic, bandgap narrowing

PACS: 61.05.cp, 71.15.Mb, 71.20.Nr, 72.80.Ga **DOI:** 10.1088/1674-1056/25/2/026101

1. Introduction

Layered Cu-based oxychalcogenides have received considerable attention due to their promise in areas including transparent conducting materials,[1–4] thermoelectric materials.[5–7] and photocatalysts,[8] etc. The two-dimensional (2D) nature of these compounds, the $(CuCh_2)^{2-}$ layer in particular, is the origin of the interesting transport and optical properties. The wide applications of these compounds are mainly determined by their bandgaps which are tunable. As a narrow band gap semiconductor, BiCuSeO has high mobility originating from the Cu 3d/S 3p antibonding states and low thermal conductivity, making it a promising candidate for commercial thermoelectric applications.[5–7] Meanwhile, the isostructural quaternary oxychalcogenides *Ln*CuOS (*Ln* = La–Nd) are optically transparent in the visible region and are used as p-type transparent conducting semiconductor.[1] Other promising candidates for wide-band-gap semiconductors are those in which perovskite-type oxide layers containing d^0 or d^{10} metals separate the antifluorite-type $[Cu_2Ch_2]^{2-}$ layers. For example, $Sr_2ZnO_2Cu_2S_2$, $Sr_3Sc_2O_5Cu_2S_2$, and their derivatives have been explored in the context of viable transparent p-type conductors, with bandgaps up to 3.1 eV.[2,3] However, when the d^{10} metals in the oxide layers of $Sr_2ZnO_2Cu_2S_2$ are replaced by magnetic atoms Co or Mn and the S atoms substituted by Se, a bandgap narrowing occurred and the optical bandgaps of $Sr_2CoO_2Cu_2Se_2$ and $Sr_2MnO_2Cu_2Se_2$ were drastically decreased to 0.068 eV and 0.073 eV, respectively.[9] The reason, however, responsible for this effective bandgap narrowing is still unclear.

The bandgap widths in Cu-based oxychalcogenides are generally correlated with the electronegativity of chalcogenide, as well as the basal lattice parameter. In LaOCu*Ch* (*Ch* = S, Se, Te) system, the bandgaps decrease from 3.1 eV to 2.31 eV with reducing the electronegativity of chalcogenide from S to Te.[4] While for a given chalcogenide ions, a decrease of the basal lattice parameter from 4.067 Å to 3.879 Å in *Ln*OCuSe (*Ln* = Y and La) also results in slight narrowing of the bandgap (from 2.82 eV to 2.58 eV).[10,11] However, the bandgap narrowing observed in $Sr_2CoO_2Cu_2Se_2$ and $Sr_2MnO_2Cu_2Se_2$ is exceptional, since such a drastic narrowing effect was not observed in other nonmagnetic oxychalcogenides systems. A natural speculation then arises that the 3d electrons in the perovskite-type oxide layers might be more or less responsible for such a bandgap narrowing. Therefore, it is desirable to find a new 3d transitional metal oxysulfide to verify this speculation and study the mechanism of bandgaps narrowing in layered Cu-based oxychalcogenides. Here, we

*Project supported by the National Natural Science Foundation of China (Grant Nos. 51472266, 51202286, and 91422303), the Strategic Priority Research Program (B) of the Chinese Academy of Sciences (Grant No. XDB07020100) and the ICDD.

†Corresponding author. E-mail: shifengjin@iphy.ac.cn

© 2016 Chinese Physical Society and IOP Publishing Ltd

report the synthesis and characterization of a new layered Cu-based oxysulfides, $Ba_3Fe_2O_5Cu_2S_2$, which is isostructural to nonmagnetic $Sr_2Sc_3O_5Cu_2S_2$ without d electrons. Interestingly, compared with the wide bandgap of 3.1 eV in $Sr_2Sc_3O_5Cu_2S_2$, the optical bandgap of $Ba_3Fe_2O_5Cu_2S_2$ significantly reduced to 1.03 eV. Our theoretical calculations indicated that $Ba_3Fe_2O_5Cu_2S_2$ should be a metal without considering the effect of spins, while it becomes a narrow bandgap mott insulator if considering the spin-polarized AFM magnetic interaction. The conduction band minimum (CBM) of $Ba_3Fe_2O_5Cu_2S_2$ is comprised of the Fe 3d/O 2p states and is considerably lowered in compared with the isostructural $Sr_3Sc_2O_5Cu_2S_2$, which is responsible for the observed bandgap narrowing.

2. Material and methods

The $Ba_3Fe_2O_5Cu_2S_2$ sample was prepared by the reaction of BaO (99.9%), FeO (99.9%), Cu (99.99%), and S (99.999%) powders in stoichiometric ratio. Reagents were mixed together and sealed inside an evacuated quartz tube. The sealed quartz tube was heated slowly to 1123 K and held at this reaction temperature for 24 h before furnace-cooling to room temperature. Powder x-ray diffraction (PXRD) was performed at room temperature using a PANalytical X'pert Pro diffractometer with Cu K_α radiation. Rietveld refinement was performed using the FULLPROF program.[12] DC magnetization $M(T)$ and Resistivity data were measured on a Physical Properties Measurement System (PPMS, Quantum Design) using powders. The diffuse reflectance spectra of the samples were measured on a UV-3600 Plus ultraviolet-visible light-near-infrared (UV-vis-NIR) spectrophotometer over the range 220 nm–2600 nm. Reflectance spectra were converted to absorbance expressed as $F(R)$ using the Kubelka–Munk function. The first principles calculations were performed using the CASTEP program.[13] The generalized gradient approximation (GGA) in the form of the Perdew–Burke–Ernzerhof was chosen to solve the exchange-correlation potentials.[14] The ultrasoft pseudopotential with a plane-wave energy cutoff of 380 eV and a Monkhorst Pack k-point separation of 0.04 $Å^{-1}$ in the reciprocal space were used for all the calculations.[15] We employed the "LDA + U" (LDA: local density approximation) correction with $U = 5$ eV for the Fe-3d electrons.[16,17]

3. Results and discussion

The room temperature PXRD pattern of the $Ba_3Fe_2O_5Cu_2S_2$ sample was shown in Fig. 1. All diffraction peaks of $Ba_3Fe_2O_5Cu_2S_2$ can be well indexed on a tetragonal cell (space group $I4/mmm$) with lattice parameters $a = 3.9995(1)$ Å and $c = 27.6873(3)$ Å. The structure of $Sr_3Fe_2O_5Cu_2S_2$[18] was used as a starting model for the Rietveld refinement against the raw data. The agreement factors of final Rietveld refinement are $R_p = 3.47\%$, $R_{wp} = 5.02\%$, and $\chi^2 = 3.57$, indicating the correct adoption of the starting model. The refinement results are summarized in Table 1. The final crystal structure is shown in the inset of Fig. 1, which is isostructural to $Sr_3Fe_2O_5Cu_2S_2$. The structure of $Ba_3Fe_2O_5Cu_2S_2$ is built up by alternatively stacking $[Cu_2S_2]^{2-}$ layers and iron perovskite oxide $[(FeO_2)(BaO)(FeO_2)]^{2-}$ layers along the c axis that are separated by barium ions. It is worth noting that the Fe^{3+} cation is fivefold coordinated by a square-pyramidal arrangement of oxygen rather than a square-planar arrangement. For all the known layered CuCh-based compounds with perovskite oxide sheets, the cations in perovskite oxide sheets locate a square pyramidal or a square planar oxygen coordination geometry. From the bond valence arguments, we inferred that the cation locates a square pyramidal oxygen coordination geometry if its valence is +3;[3,18–21] otherwise the cation locates a square-planar oxygen coordination geometry if its valence is less than

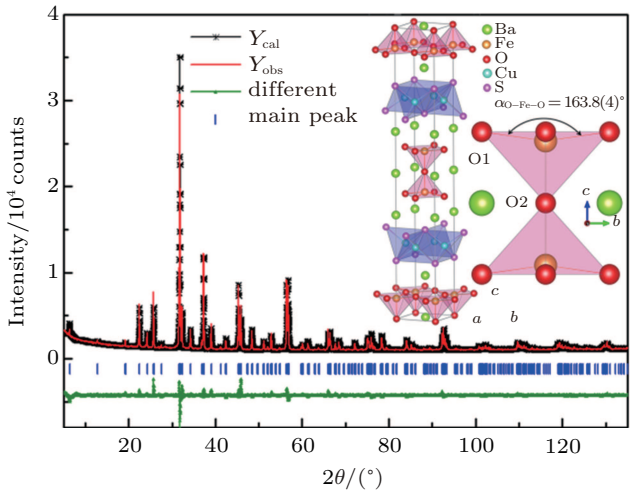


Fig. 1. (color online) PXRD pattern collected from the $Ba_3Fe_2O_5Cu_2S_2$ sample and the Rietveld refinement profiles.

Table 1. Room-temperature crystallographic data for $Ba_3Fe_2O_5Cu_2S_2$.

$Ba_3Fe_2O_5Cu_2S_2$				
Crystal system	Tetragonal			
Space group	$I4/mmm$ (No. 139)			
a/Å	3.9995(1)			
c/Å	27.6873(3)			
V/Å^3	442.884(8)			
Atomic positions	x	y	z	U_{iso}/100 Å^2
Ba1(2b)	1/2	1/2	0	0.33(8)
Ba2(4e)	1/2	1/2	0.14326(5)	0.91(6)
Fe(4e)	0	0	0.07020(16)	1.55(11)
O1(8g)	1/2	0	0.0805(3)	0.887(3)
O2(2a)	0	0	0	0.633(5)
Cu(4d)	1/2	0	1/4	0.830(5)
S(4e)	0	0	0.19982(19)	0.89(20)
Coordination				
$\alpha_{O1-Fe-O1}$/(°)	163.8(4)			
α_{S-Cu-S}/(°)	110.419			
Agreement factors				
				$R_p = 0.0347$
				$R_{wp} = 0.0502$

+3.[20,22–25] The relationship between cation positions and the bond valence was also found in $YBa_2Cu_3O_{7-x}$, where the Cu^{2+} and Cu^{3+} cations preferentially occupy square pyramidal and square planar sites, respectively.[26]

Figure 2(a) shows the temperature-dependent susceptibility $\chi(T)$ of $Ba_3Fe_2O_5Cu_2S_2$ measured under a magnetic field strength of 2000 Oe (1 Oe = 79.5775 A·m^{-1}). The $\chi(T)$ curve in high-T range of 146 K–290 K can be fitted well by the Curie–Weiss law $\chi = \chi_0 + c/(T-\theta)$, where C and θ are the Curie constant and the Weiss temperature, respectively. The fitted parameters χ_0, C, and θ are 0.0125 emu·Oe^{-1}·mol^{-1}, 9.18419 emu·K·Oe^{-1}·mol^{-1} and −504 K, respectively. The effective magnetic moment $\mu_{\rm eff}$ is determined to be 6.05(1) $\mu_{\rm B}$, which is in agreement with the value of 5.92 $\mu_{\rm B}$ expected for the high spin d^5 configuration of Fe^{3+}.[27] The negative value of θ indicates that the dominant magnetic interactions in the compound are antiferromagnetic (AFM). The sharp peak at 121 K indicates an AFM transition. Also, the dependence of isotemperature magnetization on magnetic field H shows that magnetization$M$ is nearly proportional to H even down to 10 K, with minor hysteresis possibly due to trace impurities that undetectable in PXRD. The Curie–Weiss-like upturn at low temperatures is presumably due to the paramagnetic impurities as in $Ba_2CoO_2Ag_2Se_2$.[28]

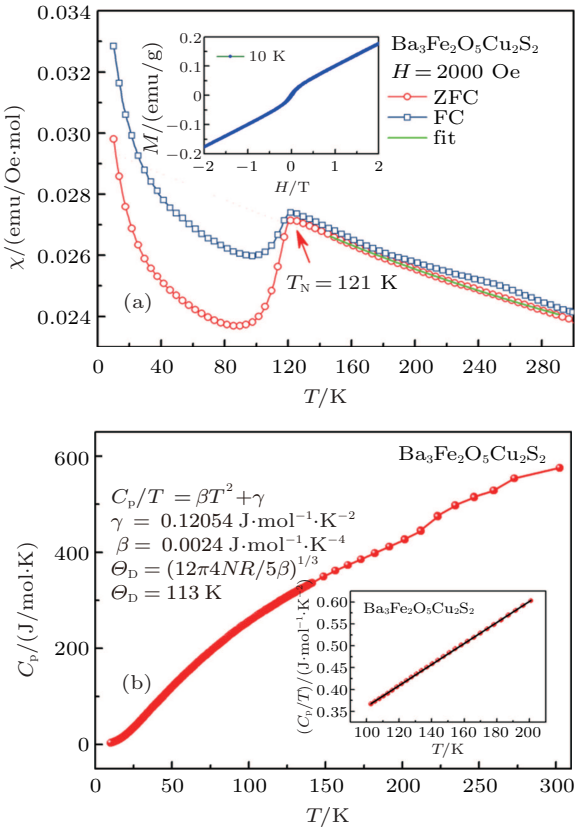


Fig. 2. (color online) (a) Zero field cooling (ZFC) and field cooling (FC) $\chi(T)$ data taken in an applied field of 2 kOe. The fit to the Curie–Weiss law is shown as a green line. Inset: the M–H curves at 10 K. (b) Temperature dependence of specific heat $C_{\rm p}(T)$ of $Ba_3Fe_2O_5Cu_2S_2$ from 10 K to 300 K.

The heat capacity versus T at constant pressure $C_{\rm p}$ at $H = 0$ was plotted in Fig. 2(b). There is no clear anomaly at AFM transition temperature $T_{\rm N}$ of 121 K, despite the relatively sharp magnetic ordering transition observed by magnetization. Analyses of $C_{\rm p}(T)$ curves commonly yield magnetic entropies above $T_{\rm N}$ smaller than expected for the paramagnetic state, mostly due to short range magnetic correlations at $T > T_{\rm N}$ and the difficulty of separating the phonic contrubution from the spin-wave specific heats at $T < T_{\rm N}$. This phenomenon was also observed in $LaCrSb_3$[29] and $Sr_2Mn_3As_2O_2$.[30] As shown in the inset of Fig. 2(b), $C_{\rm p}(T)/T$ versus T^2 shows a perfect linear characteristic at low temperature (10 K∼15 K). It is fitted by the expression $C_p/T = \gamma + \beta T^2$, where γ is the Sommerfeld coefficient. The fitted parameters β and γ are 0.0024 J·mol^{-1}·K^{-4} and 0.1205 J·mol^{-1}·K^{-2}, respectively. According to the formula $\Theta_{\rm D} = (12\pi 4NR/\beta)^{1/3}$, the Debye temperature $\Theta_{\rm D}$ is estimated to be about 113 K.

Figure 3(a) gives the variation of resistivity with temperature for $Ba_3Fe_2O_5Cu_2S_2$. It exhibits a semiconducting behavior from 55 K to 300 K. The $\rho(T)$ obeys the thermally activated behavior $\rho = \rho_0 \exp(E_{\rm a}/k_{\rm B}T)$, where $E_{\rm a}$ is the activation energy. The obtained $E_{\rm a}$ is 0.011 eV, which is much smaller than that of Ca_2FeO_3CuS (0.19 eV).[19] For a magnetic semiconductor, electrical conduction results mainly from electron-hopping between adjacent spin sites. Thus, the longer Fe–Fe and Fe–O distances in $Ba_3Fe_2O_5Cu_2S_2$ result in a weaker overlapping integral between the electron-wave-function at the adjacent Fe^{3+} sites for hopping conduction, which explains the small electrical conductivity observed than that of Ca_2FeO_3CuS.

The UV-vis-NIR diffuse reflectance spectra of $Ba_3Fe_2O_5Cu_2S_2$ were displayed in Fig. 3(b) In the $F(R)$ versus $h\nu$ plots, the absorption edge can be deduced via the straightforward extrapolation method. The optical band gap is estimated to be about 1.03 eV, which is consistent with the gray-black color of the material. The optical band gap of $Ba_3Fe_2O_5Cu_2S_2$ is much larger than its activation energy value of 0.011 eV deduced from resistivity. The disparity between the two energy values is understandable since the activation energy $E_{\rm a}$ extracted from the resistivity of the polycrystalline samples may be resulted from shallow impurity levels located below (above) conduction (valence) band.

The electrical properties and bandgaps of typical compounds with and without magnetic atoms were summarized and compared in Table 2, where the majority of reported Cu-based oxychalcogenides are semiconductors. A few compounds present metallic behavior because less than two electrons are transported to $[Cu_2Ch_2]^{2-}$ layer so that their valance bands are not fully filled.[32] It is found that the bandgaps of the titled compound and the $Sr_2MO_2Cu_2Se_2$ (M = Co, Mn) are much less than the typical band-gaps 2 eV–3 eV of other reported oxychalcogenide semiconductors that without

3d electrons.[1–3,9,10,33] Thus, it is speculated that the magnetic atoms in the compounds have a significant effect on the electronic structure.

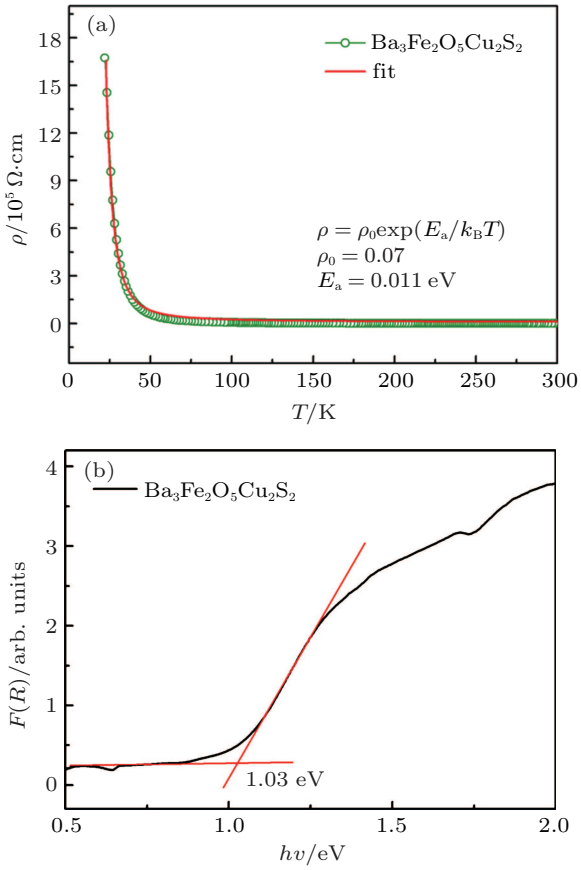


Fig. 3. (color online) (a) Temperature dependence of the resistivity $\rho(T)$ of the $Ba_3Fe_2O_5Cu_2S_2$ with $H = 0$. The red line is the fitting results of $\rho(T)$ using thermal activation model. (b) UV-vis-NIR diffuse reflectance spectrum of $Ba_3Fe_2O_5Cu_2S_2$.

Table 2. Several typical Cu*Ch*-based compounds and their electrical properties.

Compound	Ground state	E_g/eV
HgOCuSe[31]	metallic	–
$Bi_2YO_4Cu_2Se_2$[32]	metallic	–
LaOCuS(Se)[1,33]	semiconducting	3.1(2.8)
YOCuSe[10]	semiconducting	2.58
Sr_2GaO_3CuS[2]	semiconducting	2.6
Sr_2InO_3CuS[2]	semiconducting	2.3
$Sr_2ZnO_2Cu_2S_2$[2]	semiconducting	2.7
$Sr_3Sc_2O_5Cu_2S_2$[3]	semiconducting	3.1
$Sr_2MnO_2Cu_2Se_2$[9]	semiconducting	0.073
$Sr_2CoO_2Cu_2Se_2$[9]	semiconducting	0.068
$Ba_3FeO_5Cu_2S_2$	semiconducting	1.03

Electronic structures of the titled compound were calculated based on the first principles calculations considering the two cases of the nonmagnetic structure and the spin-polarized structure. A nonmagnetic calculation was first performed where the spins of the magnetic atoms are not considered and the calculated band structure along the high-symmetry k lines was showed in Fig. 4(a). The bands located from 0 eV to 2 eV basically come from the hybridization of O 2p and Fe 3d states The bands located from −2 eV to 0 eV are contributed by Cu 3d and S 3p states besides the O 2p and Fe 3d states, while the Cu 4s bands distribute above 2 eV. The obtained band structure for $Ba_3Fe_2O_5Cu_2S_2$ exhibits a metal feature, which is inconsistent with the previous result of resistivity measurements.

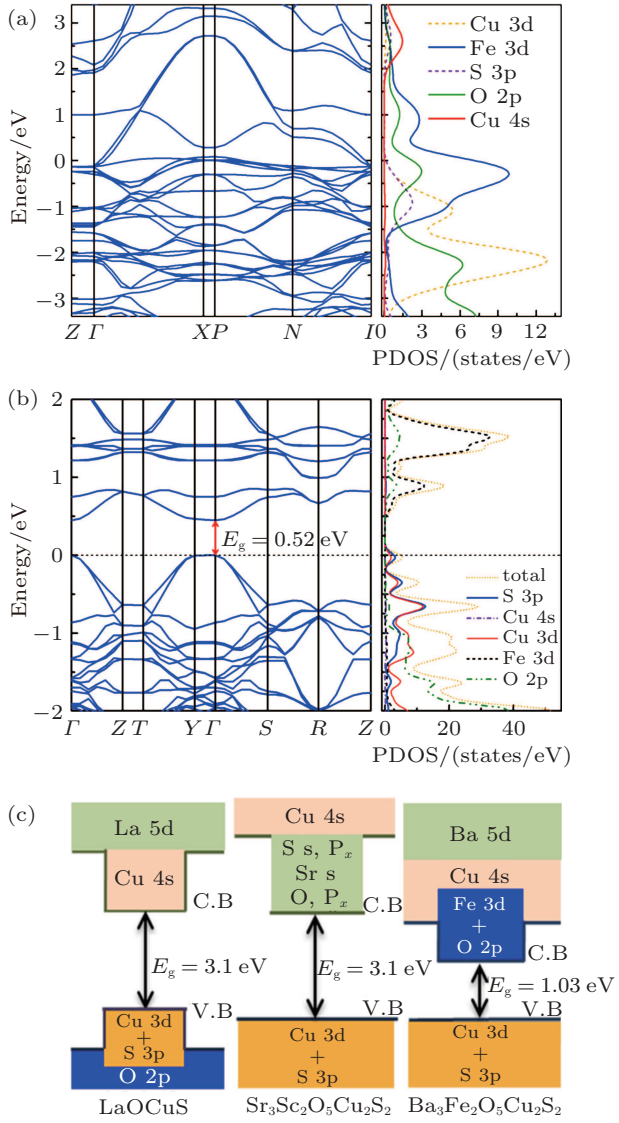


Fig. 4. (color online) Band structure (left) and total/atom resolved partial density of states (PDOS) (right) near the Fermi energy for (a) nonmagnetic $Ba_3Fe_2O_5Cu_2S_2$ and (b) antiferromagnetic $Ba_3Fe_2O_5Cu_2S_2$ with $U = 5$ eV. (c) The schematic diagrams of band structure for LaOCuS, $Sr_3Sc_2O_5Cu_2S_2$ and antiferromagnetic $Ba_3Fe_2O_5Cu_2S_2$, respectively.

Then, a spin-polarized calculation was performed by using LDA + U method with $U = 5$ eV. A G-type AFM structure was adopted for $Ba_3Fe_2O_5Cu_2S_2$ as reported in $Sr_3Fe_2O_5Cu_2S_2$.[34] As shown in Fig. 4(b), both the minimal-energy state in the conduction bands and the maximal-energy state in the valence bands are located at the Γ point ($k = 0$), indicating that $Ba_3Fe_2O_5Cu_2S_2$ is a direct band-gap semiconductor with a bandgap of 0.52 eV. The underestimation relative to the experimentally measured optical band gap of 1.03 eV is on account of the well-known problem that LDA + U calculations always give underestimated band gaps.[35] The spin-

polarized atom-resolved density of states are shown in the right panel of Fig. 4(b). The valence band maximum, which is mostly contributed by the Cu 3d states and S 3p states, is similar to quaternary oxychalcogenides[1,10,33] and multilayered mixed-metal oxychalcogenides,[2,3,9] while the conduction band minimum is different even between the isostructural compounds. As schematically diagrammed in Fig. 4(c), the CBM of $Ba_3Fe_2O_5Cu_2S_2$ is dominated by the Fe 3d and O 2p states, while the CBM of the isostructural compound $Sr_3Sc_2O_5Cu_2S_2$ is dominated by sulfur s and p_z states, Sr s states and O p_x states,[36] and the CBM of LaOCuS is occupied by Cu 4s orbitals.[37] As shown in Fig. 5, the CBM of $Sr_3Fe_2O_5Cu_2S_2$ and Ca_2FeO_3CuS compounds are also comprised of the Fe 3d/O 2p states through the first principles calculations. They are direct band-gap semiconductors with a bandgap of 1.25 eV and 1.35 eV, respectively. The CBM that are comprised of the Fe 3d/O 2p states lie at much lower energy compared with nonmagnetism compound $Sr_3Sc_2O_5Cu_2S_2$, which result in a bandgap narrowing. The band gaps can be divided into two regimes in terms of gap values: the layered Cu*Ch*-based compounds without magnetic cations fall in Regime I (band gap range from 2 eV to 3 eV); the layered Cu*Ch*-based compounds with magnetic cations fall in Regime II (band gap range from 0 eV to ∼1 eV). Therefore, the magnetism in perovskite oxide sheets predominantly affects the conduction band minimum and results in a much narrower band gap.

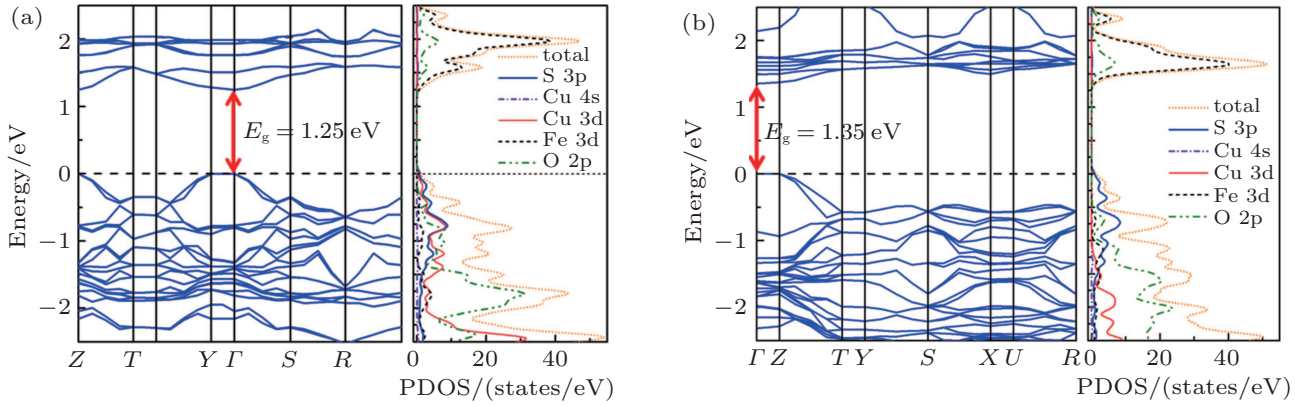


Fig. 5. (color online) Band structure (left) and total/atom resolved partial density of states (PDOS) (right) near the Fermi energy for antiferromagnetic $Sr_3Fe_2O_5Cu_2S_2$ (a) and Ca_2FeO_3CuS (b) with $U = 5$ eV.

4. Conclusion

In summary, a new layered oxychalcogenides compound $Ba_3Fe_2O_5Cu_2S_2$ was synthesized and the underlying bandgap narrowing mechanism is revealed by experimental and DFT calculations. Refinement of powder x-ray diffraction data shows that its structure is built up by alternatively stacking $[Cu_2S_2]^2$ layers and iron perovskite oxide $[(FeO_2)(BaO)(FeO_2)]^{2-}$ layers along the *c* axis that are separated by barium ions, with Fe^{3+} cation locates in a square-pyramidal oxygen coordination geometry. From the bond valence arguments we inferred that in layered Cu*Ch*-based oxychalcogenides with perovskite oxide sheets the +3 cationsoccupy square pyramidal sites while the cations with less than +3 locate square planar sites. The optical bandgap of $Ba_3Fe_2O_5Cu_2S_2$ is about 1.03 eV, much smaller than the reported nonmagnetic oxychalcogenides. The magnetic susceptibility and transport measurements indicate that $Ba_3Fe_2O_5Cu_2S_2$ is an AFM ordering semiconductor with a Néel temperature of 121 K. Electronic structures of a nonmagnetic calculations present metallic behavior, while for a spin-polarized calculation on AFM magnetic structure the results show that $Ba_3Fe_2O_5Cu_2S_2$ has a considerable bandgap opened and CBM that are comprised of the Fe 3d/O 2p states lie at much lower energy compared with isostructural $Sr_3Sc_2O_5Cu_2S_2$, which result in a bandgap narrowing.

References

[1] Ueda K, Inoue S, Hirose S, Kawazoe H and Hosono H 2000 *Appl. Phys. Lett.* **77** 2701

[2] Ueda K, Hirose S, Kawazoe H and Hosono H 2001 *Chem. Mater.* **13** 1880

[3] Liu M L, Wu L B, Huang F Q, Chen L D and Chen I W 2007 *J. Appl. Phys.* **102** 116108

[4] Liu M L, Wu L B, Huang F Q, Chen L D and Ibers J A 2007 *J. Solid State Chem.* **180** 62

[5] Zhao L D, Berardan D, Pei Y L, Byl C, Pinsard-Gaudart L and Dragoe N 2010 *Appl. Phys. Lett.* **97** 092118

[6] Li J, Sui J, Pei Y, Barreteau C, Berardan D, Dragoe N, Cai W, He J and Zhao L D 2012 *Energ. Environ. Sci.* **5** 8543

[7] Hiramatsu H, Yanagi H, Kamiya T, Ueda K, Hirano M and Hosono H 2008 *Chem. Mater.* **20** 326

[8] Jia Y, Yang J, Zhao D, Han H and Li C 2014 *J. Energ. Chem.* **23** 420

[9] Jin S F, Chen X L, Guo J G, Lei M, Lin J J, Xi J G, Wang W J and Wang W Y 2012 *Inorg. Chem.* **51** 10185

[10] Ueda K, Takafuji K, Yanagi H, Kamiya T, Hosono H, Hiramatsu H and Hirano M 2007 *J. Appl. Phys.* **102** 113714

[11] Clarke S J, Adamson P, Herkelrath S J C, Rutt O J, Parker D R, Pitcher M J and Smura C F 2008 *Inorg. Chem.* **47** 8473

[12] Rodríguez-Carvajal 1990 *Satellite Meeting on Powder Diffraction of the XV Congress of the IUCr*, Toulouse, France, 1990

[13] Clark S J, Segall M D, Pickard C J, Hasnip P J, Probert M J, Refson K and Payne M C 2005 *Z. Kristallogr.* **220** 567

[14] Perdew J P, Burke K and Ernzerhof M 1996 *Phys. Rev. Lett.* **77** 3865

[15] Monkhorst H J and Pack J D 1976 *Phys. Rev. B* **13** 5188
[16] Vladimir I A, Aryasetiawan F and Lichtenstein A I 1997 *J. Phys.: Condens. Matter* **9** 767
[17] Kutepov A, Haule K, Savrasov S Y and Kotliar G 2010 *Phys. Rev. B* **82** 045105
[18] Zhu W J and Hor P H 1997 *J. Solid State Chem.* **134** 128
[19] Charkin D O, Sadakov A V, Omel'yanovskii O E and Kazakov S M 2010 *Mater. Res. Bull.* **45** 2012
[20] Zhu W J and Hor P H 2000 *J. Solid State Chem.* **153** 26
[21] Zhu W J and Hor P H 1997 *Inorg. Chem.* **36** 3576
[22] Zhu W J, Hor P H, Jacobson A J, Crisci G, Albright T A, Wang S H and Vogt T 1997 *J. Am. Chem. Soc.* **119** 12398
[23] Otzschi K, Ogino H, Shimoyama J I and Kishio K 1999 *J. Low. Temp. Phys.* **117** 729
[24] Zhu W J and Hor P H 1997 *J. Solid State Chem.* **130** 319
[25] Gál Z A, Rutt O J, Smura C F, Overton T P, Barrier N, Clarke S J and Hadermann J 2006 *J. Am. Chem. Soc.* **128** 8530
[26] David W I F, Harrison W T A, Gunn J M F, Moze O, Soper A K, Day P, Jorgensen J D, Hinks D G, Beno M A, Soderholm L, Capone Ii D W, Schuller I K, Segre C U, Zhang K and Grace J D 1987 *Nature* **327** 310
[27] Pan Y W, Zhu P W and Wang X 2015 *Chin. Phys. B* **24** 017503
[28] Zhou T T, Wang Y M, Jin S F, Li D D, Lai X F, Ying T P, Zhang H, Shen S J, Wang W J and Chen X L 2014 *Inorg. Chem.* **53** 4154
[29] Granado E, Martinho H, Sercheli M S, Pagliuso P G, Jackson D D, Torelli M, Lynn J W, Rettori C, Fisk Z and Oseroff S B 2002 *Phys. Rev. Lett.* **89** 107204
[30] Nath R, Garlea V O, Goldman A I and Johnston D C 2010 *Phys. Rev. B* **81** 224513
[31] Kim G, Cheon M, Park I, Ahmad D and Kim Y 2011 arXiv: 1105.5868
[32] Tan S G, Shao D F, Lu W J, Yuan B, Liu Y, Yang J, Song W H, Lei H and Sun Y P 2014 *Phys. Rev. B* **90** 085144
[33] Ueda K, Hosono H and Hamada N 2005 *J. Appl. Phys.* **98** 043506
[34] Cario L, Lafond A, Morvan T, Kabbour H, André G and Palvadeau P 2005 *Solid State Sci.* **7** 936
[35] Scanlon D O, Walsh A, Morgan B J, Watson G W, Payne D J and Egdell R G 2009 *Phys. Rev. B* **79** 035101
[36] Scanlon D O and Watson G W 2009 *Chem. Mater.* **21** 5435
[37] Ueda K, Hiramatsu H, Hirano M, Kamiya T and Hosono H 2006 *Thin Solid Films* **496** 8